Carbon balance, atmospheric CO_2 variability and meridional CO_2 flux distribution using forward and inverse models

Prabir K. Patra[1], Thomas J. Conway[2], Yasunori Tohjima[3], Kenneth Masarie[2], Kazuyuki Miyazaki[1], Masayuki Takigawa[1], Shamil Maksyutov[1,3] and Takakiyo Nakazawa[1,4]

1. Research Institute for Global Change/JAMSTEC, Yokohama, Kanagawa 236 0001, Japan

2. NOAA Earth System Research Laboratory, Boulder, CO 80305-3337, USA

3. National Institute for Environmental Studies, Tsukuba, Ibaraki 305-8506, Japan

4. Tohoku University, Sendai 980 8578, Japan

Full Addresses:

T. J. Conway, K. Masarie
Earth System Research Laboratory, National Oceanic and Atmospheric Administration, 325 Broadway, Boulder, CO 80305-3337, USA

S. Maksyutov, Y. Tohjima
Center for Global Environmental Research, National Institute for Environmental Studies, 16-2 Onogawa, Tsukuba, Ibaraki 305-8506, Japan

K. Miyazaki, P. K. Patra, M. Takigawa
Research Institute for Global Change, Japan Agency for Marine-Earth Science and Technology, 3173-25 Showa-machi, Yokohama, Kanagawa 236 0001, Japan (e-mail: prabir@jamstec.go.jp)

T. Nakazawa,
Center for Atmospheric and Oceanic Studies, Graduate School of Science, Tohoku University, 6-3 Aoba, Sendai, 980-8578, Japan

---

Last modified: 15 June 2010

Abstract.

Ways to evaluate the quality of inverse model estimated fluxes of carbon dioxide (CO_2) are being developed in this work. A chemistry-transport model and two sets of inverse model-estimated surface fluxes are used for simulating CO_2 in the atmosphere for the period 1984-2006. The results are compared with an observations-based data product and flask observations at surface sites and aircraft profiles. The cumulative growth rates are reproduced within 0.3 ppm at several sites with data coverage over the full analysis period, and the cumulative increase of the atmospheric burden of CO_2 is estimated to be 82.2 PgC. The airborne fraction of CO_2 was lower by about 9% in the 1990s compared to an average value of 59% for the 1980s and 2000s. The spatial gradients between sites are well represented by the model, commonly within 1.0 ppm at the remote sites, indicating the realistic representation of surface flux gradients. The forward simulation is able to capture the CO_2 seasonal cycle and growth rate variability at most of the 139 sites considered here with at least 6 years of data coverage over the 1996-2005 period. However, further detailed comparison of model and observed CO_2 latitudinal gradient suggests that mean carbon uptake, derived by inversion of CO_2 data using multiple forward models, is overestimated in the northern hemisphere with respect to the southern hemisphere by 0.46 PgC yr^{-1}. A combination of forward transport and flux inversion model results suggests net carbon fluxes of -2.0, 1.6 and -2.4 PgC yr^{-1} (excluding fossil fuel consumption) across the earth's surface in the 90-15^{o}N, 15^{o}N-15^{o}S, and 15-90^{o}S latitude bands, respectively, during 2000-2002. These flux gradients remained fairly constant across the span our analysis of 1984-2006.

1. Introduction

The contribution of atmospheric CO_2 to global warming is the highest among all anthropogenically-produced gases, and direct measurements have been started in the late 1950s [Keeling et al., 1989 and references therein]. However, it is still challenging to account for the budget of CO_2 in the earth system. The partitioning of land and oceanic sinks still have large uncertainty [since Tans et al., 1990; Keeling 1996a], the amount of emission due to fossil fuel burning that remains in the atmosphere, the so called airborne fraction (AF) or residual flux as defined here, can be debated [Canadell et al., 2007; Khatiwala et al., 2009], and bias exists in the simulated atmospheric-CO_2 latitudinal gradient [Denning et al., 1995]. Thus the estimation of CO_2 fluxes (sink: negative flux; source: positive flux into the atmosphere) at regional/continental/global scales has been of interest for understanding the carbon cycling in the earth system and to develop effective policies for mitigating CO_2 increase in the atmosphere. Atmospheric observations and forward transport model simulations have been shown to be useful for deriving surface fluxes at regional scales and for multiple years by inverse modeling techniques [e.g., Rayner et al., 1999]. However, large uncertainty in the flux estimates is prevalent due to the forward transport model error. This situation led to the TransCom-3 CO_2 flux inversion project involving multiple forward model simulations, which concluded that the flux estimation uncertainty within the inverse model (due to sparse data coverage) is greater than the flux uncertainty due to forward model transport error [e.g., Gurney et al., 2004]. Major challenges remain relatively unexplored regarding how to validate the mean/net fluxes as estimated by various inverse/assimilation/process models.

Studies show that the CO_2 seasonal cycle and growth rates at Mauna Loa Observatory (MLO) respond to interannual, decadal or inter-decadal climate variability [Keeling et al., 1996; Patra et al., 2005; Buermann et al., 2007], and the increase in concentration difference between MLO and South Pole Observatory (SPO) is due to greater fossil emission increase in the Northern Hemisphere (NH) than in the Southern Hemisphere (SH). Since the exponential decay time of source signal difference between the two hemispheres is about 1.3±0.1 years, referred to as inter-hemispheric exchange time [Geller et al., 1997], a positive SH to NH gradient in CO_2 concentration is produced because the NH is net source of CO_2 to the atmosphere [Keeling et al., 1989; Conway et al., 1994]. Because of non-negligible impact of diurnal, synoptic or interannual transport on CO_2 variability [Law et al., 2008; Patra et al., 2008; Higuchi et al., 2002], inter-annually varying transport should be used for multi-year flux inversion studies. However, the CO_2 source/sink inversion using multiple forward models and interannually varying winds has not been done systematically covering several decades due to limitation in computational resources. On the other hand, it is suggested that derivation of flux interannual variability is not strongly dependent on forward model selection under the same inverse model setup [Baker et al., 2006]. Therefore, we will introduce interannual variability of CO_2 flux derived using one forward transport model on top of an average flux seasonal cycle obtained using multiple forward models.

One of our aims here is to construct CO_2 surface fluxes with realistic latitudinal gradient and interannual variability for simulating spatial gradients and temporal variability in atmospheric CO_2 over several decades. An atmospheric general circulation model-based chemistry-transport model (ACTM) has been employed to analyze the CO_2 concentration gradients across latitude, longitude and altitude in relation to surface fluxes and atmospheric transport. Additionally, forward transport model simulations with realistic surface fluxes can be used to create 3-dimensional data products of atmospheric constituents similar to existing meteorological reanalysis. Recently, Carbon Tracker has provided such a field for CO_2, but limited to the 2000s probably due to the high computational demands of their modeling system [Peters et al., 2007], and this study extends the period back to the early 1980s (similar to Chavallier et al., 2011). Moreover, the model-observation mismatches are utilized here to obtain critical information on accuracy of the latitudinal distribution of surface flux, and later used as a measure to define quality of an inverse model estimated flux when the ACTM forward transport is employed. Important to note here that the model-observation mismatch statistics obtained in this study are using forward simulation of inverse model predicted fluxes. In the TransCom experiment [Gurney et al., 2004], the northern terrestrial CO_2 uptake varied widely (in the range of 0.0 to 4.0 Pg-C yr^{-1}) depending on the forward transport model, even though the mismatch statistics between a priori and predicted data corresponding to different transport models were fairly similar (mostly within ±1.0 ppm). Thus we believe simulating inversion fluxes by a forward transport model with relatively unbiased transport properties and then comparing with observed CO_2 concentrations will lead to better insight about the accuracy of inversion fluxes than those obtained from the a posteriori data.

2. Methods

The Center for Climate System Research/National Institute for Environmental Studies/Frontier Research Center for Global Change (CCSR/NIES/FRCGC) atmospheric general circulation model [Numaguti et al., 1997], nudged towards the horizontal winds and temperature from the National Center for Environmental Prediction/Department of Energy Reanalysis 2, has been adopted for chemistry-transport simulations of long-lived gases in the atmosphere for the period 1979-present [e.g., Patra et al., 2009]. It has been shown that the sulphur hexaflouride (SF_6; an inert chemical tracer) interhemispheric gradients and estimated interhemispheric mass exchange time of 1.2 years obtained by ACTM are in agreement with those from observations [Patra et al., 2009], and have also been validated using a larger number of sites in a multi-model framework [Law et al., 2008]. The performance of ACTM for simulating the CO_2 diurnal cycle and synoptic variability has been evaluated to be satisfactory under the TransCom continuous experiment [Law et al., 2008; Patra et al., 2008]. Thus ACTM has been selected for forward transport simulation of all inversion fluxes and one case of flux inversion.

The monthly mean seasonal fluxes (cyclostationary), averaged across the 12 TransCom-3 models, for the 11 land and 11 ocean (22 in total) regions are obtained using inversion [Gurney et al., 2004]. This inversion is conducted using the GLOBALVIEW-CO_2 at 87 sites with less than 30% missing data in the smoothed time series over the period of 2000-2002 [GLOBALVIEW-CO_2, 2009], as opposed to 75 sites for the 1992-1996 period in TransCom-3. The time period of 2000-2002 is selected [as in Patra et al., 2006], which did not experience any of the extreme climate anomalies, such as the Mount Pinatubo volcanic eruption in 1991, the El Nino even in 1997/1998 or the boreal forest fires in 1996, 1998, 2003. This flux is referred to as INV22_CYC [Please refer to the Supplementary Materials, Fig. S1]. The CO_2 signals from the fossil fuel emissions distribution representing the year 1995 [Brenkert, 1998; scaled to a global total of 6.6 PgC yr^{-1}], terrestrial flux from the CASA (Carnegie Ames Stanford Approach) biogeochemical model [Randerson et al., 1997] and the sea-to-air oceanic fluxes for climatological mean conditions normalized to 1995 [Takahashi et al., 2002] are presubtracted as described in TransCom inversion intercomparison protocol [Gurney et al., 2000].

Next we solve for interannually varying fluxes across 1979-2007 for 42 land and 22 ocean regions using only the NIES/FRCGC chemistry-transport model (CTM), which is driven by interannually varying winds [Patra et al., 2005; Maksyutov et al., 2008 and references therein]. The fossil fuel presubtraction for this inversion is based on the interannually varying distribution and strength of emissions prepared at the Oak Ridge National Laboratory (ORNL) [Andres et al., 2010], while the terrestrial and oceanic presubtractions are identical to INV22_CYC. The INV22_IAV64 fluxes are estimated using CO_2 data at 26 sites (Table S1) and 80 sites (Fig. S1) for the period 1979-1991 and 1992-2007, respectively. Different networks are selected to avoid long gaps in observation record for the respective inversion periods. The average seasonal cycles are computed for each of the 64 inverse model regions over the period of our analysis 1984-2006 (first few years and last one year of inversion are discarded). These averages are subtracted off of the originally estimated monthly fluxes to calculate CO_2 flux anomalies.

These anomalies have been added back on to the 2000-2002 seasonal cycle from the previous inversion (i.e., INV22_CYC) for preparing interannually varying flux (referred to as INV22_IAV64). Thus the ACTM forward simulation using INV22_IAV64 flux will produce similar latitudinal CO_2 concentration gradients as that due to INV22_CYC, but the interannual CO_2 variations are expected to be better reproduced.

A third set of fluxes, designated "INV64_CYC", is also used (see Section 3.4). These fluxes were generated by an inversion similar to that which gave the INV22_CYC fluxes, but performed only with the ACTM forward transport (rather than all 12 TransCom3 models), and solving for 64 instead of 22 regions. The presubtracted signal for fossil fuel emission is prepared differently as 0.2 x EDGAR4 + 0.8 x ORNL (both scaled to CDIAC global totals), while the terrestrial and oceanic presubtraction fluxes are identical to the other two inversions. The use of EDGAR4 or ORNL fossil fuel emission separately do not produce significantly different latitudinal gradient in zonal aggregated inversion fluxes, although differences are visible at the subcontinental scale regions (cf. Fig. S1). A summary of how the surface CO_2 fluxes were generated is given in Table 1.

The first two sets of fluxes described above were run through the ACTM transport model in separate forward simulations, using annual-mean fossil fuel emission distribution at $1^o \times 1^o$ horizontal resolution for the period of 1980-2005 are taken from EDGAR4 (Emission Database for Global Atmospheric Research, version 4.0; http://www.jrc.europa.eu, 2009). Before adding to the inversion based land and ocean carbon fluxes, the EDGAR4 emissions are scaled to comply with global totals available at the Carbon Dioxide Information and Analysis Center (CDIAC) [Boden et al., 2009]. This yields a global total of 6.7 PgC yr^{-1} for the year 2000 – a magnitude similar to that is used in INV22_CYC. The EDGAR4 emission distribution for 2005 is repeated for the later years. The first five years (1979-1983) of ACTM simulations are considered as model spin-up and the time series for the period 1984-2006 are analyzed. All the fluxes used for forward and inverse modeling does not include diurnal cycles, and thus the simulated daytime CO_2 concentration over the continental regions will be biased towards a higher value during the periods of high ecosystem activity.

The simulated CO_2 spatial and temporal variations are compared at a variety of measurement sites, such as the continental, coastal, remote and aircraft profiles (Table S1). The three letter GLOBALVIEW-CO_2 site codes are used in the text. The 3-hourly average model output is sampled for site-specific 1300 to 1500 local time, and then monthly mean values are calculated for the daily-interval model and weekly-interval GLOBALVIEW-CO_2 time series. A sensitivity analysis is conducted using the NOAA Earth System Research Laboratory (ESRL) event-based observations at 29 long-term monitoring sites. Model output is sampled at the time and day of flask air sampling (unflagged data only). For calculating seasonal cycles and growth rates, a digital filtering technique (Nakazawa et al., 1997) is applied to each time series. The digital filtering technique separates the long-term trend by passing the time series through a low-pass filter with cutoff period of 36 months, and 3 harmonics are fitted to the residual (original –long term trend) time series to obtain the seasonal cycle. The time derivative of the long-term trend is defined as growth rate. The model results are evaluated using Pearson's moment correlation coefficient, r, with respect to the observational data, and normalized standard deviation (NSD; defined as the ratio of 1σ values from model and observations).

3. Results and Discussion

3.1. Airborne Fraction and CO_2 time series comparison

Figure 1a shows the global total CO_2 emissions due to fossil fuel and landuse/landuse change (LULUC), and residual fluxes that essentially remain in the atmosphere. The residual fluxes are calculated by summing the INV22_CYC or INV22_IAV64 fluxes with the assumed fossil fuel emissions. The inversion results include terrestrial, oceanic and LULUC fluxes. The cumulative residual flux of 82.9 PgC over 1984-2006 for INV22_IAV64 compares well with what is estimated from the aggregated increase in CO_2 concentration at MLO (82.2 PgC). Cumulative fossil fuel emission over the same period was 149.4 PgC. If the airborne fraction is estimated as the ratio of atmospheric increase to the fossil fuel emissions, the decadal average values range from 48 to 61% (Table 2). The airborne fractions for INV22_IAV64 flux and calculated from the MLO growth rate are found to be ~59% in 1984-1989 and 2000-2006, but lower in the period of 1990-1999 (~51%). The lower airborne fraction is most likely caused by the enhanced terrestrial ecosystem uptake as an effect of volcanic aerosols following the Mt. Pinatubo eruption in June 1991 [Gu et al., 2002; Lucht et al., 2002; Patra et al. 2005]. The INV22_IAV64 case is thus consistent with the inter-decadal variability in airborne fraction derived from the measurements, and suggests no apparent trends in the past 23 years. The interannual variability of the residual flux for the INV22_IAV64 case and the atmospheric increase derived from the MLO growth rate are in good agreement (r=0.91 for the period 1984-2006). The cumulative residual flux of 81.3 PgC over 1984-2006 for INV22_CYC case is also close to observation based result, due to the fact the average atmospheric growth rate for 2000-2002 is very close to what can be calculated for 1984-2006.

Figures 1b,c show the time series of observed and simulated atmospheric CO_2 at MLO and SPO, and concentration difference between these two sites representing the changes in the interhemispheric gradient. The increase in CO_2 concentration is reproduced by both the inversion fluxes, even though CO_2 fluxes across the land/ocean-atmosphere are assumed constant for the whole simulation period for the

INV22_CYC case, due to the increase in fossil fuel emissions. Also because the fossil fuel CO_2 net emission and emission increase are greater in the NH (4.7 PgC in 1984 to 7.3 PgC in 2006) than the SH (0.56 PgC in 1984 to 0.96 PgC in 2006), the interhemispheric gradient has increased steadily by about 1.0 ppm during the period 1984-2006. However, the ACTM simulation systematically underestimates the CO_2 concentration difference between MLO and SPO by about 0.5 ppm, except for the period 1991-1993, following the Mt. Pinatubo eruption. This suggests the modeled (INV22_CYC case) terrestrial and oceanic sink of 1.91 PgC yr^{-1} in the NH is stronger or the modeled sink of 0.88 PgC yr^{-1} in the SH is weaker than what are required for simulating the CO_2 interhemispheric gradients accurately. As mentioned earlier, the ACTM does not have any apparent bias in simulating the interhemispheric gradient in SF_6 (within 10% of the observed gradients) and in estimation of the interhemispheric exchange time [Patra et al., 2009]. If these results are taken literally, the NH-SH sink contrast of 1.03 PgC yr^{-1} should be reduced by about 0.5 PgC yr^{-1} for successful reproduction of the CO_2 concentration difference between MLO and SPO, assuming the validity of the fossil fuel emission distribution and 1.0 ppm CO_2 corresponds to 1.06 PgC in each hemisphere (1.06 factor is half of that is assumed for CO_2 emission to concentration conversion for an 1 ppm global growth rate; Fig. 1 caption). The forward simulations of inverse model derived fluxes appear promising to evaluate the quality of surface fluxes and flux change with time. Further detailed discussion will be made using the inverse model estimated fluxes for ACTM forward transport later in section 3.4.

3.2. Spatial gradients in CO_2 concentration

To elucidate the utility of forward simulation for testing the validity of surface fluxes, concentration differences between a variety of sites are explored (Fig. 2). The concentration differences between sites are mainly caused by gradients in surface fluxes and changes in meteorology with season, such as the monsoon. Generally, the ACTM simulates the features present in the GLOBALVIEW-CO_2 fairly well. The change in CO_2 concentration differences between MLO/IZO and HAT (Fig. 2e,f) with time is mainly caused by the increase in fossil fuel emission, which has apparently accelerated since the early 2000s over continental Asia [e.g., Gregg et al., 2008; Tohjima et al., 2010]. Because HAT site is located in the Chinese emission outflow region during the boreal winter-spring seasons, the CO_2 concentrations are higher than MLO (central Pacific Ocean), and thus HAT–MLO values increase for the period 2000-2005. During the boreal summer when winds at HAT are mainly from the Pacific Ocean, under the influence of the East Asian monsoon trade winds, no change in concentration difference is observed. On the contrary, HAT–IZO (Atlantic Ocean) values increased in all seasons, suggesting an overall enhancement of CO_2 concentration in the Asia-Pacific region compared to the North Atlantic region. Note that the lower increase rate for HAT–IZO and HAT–MLO concentration differences in the case of INV22_IAV64 compared to the INV22_CYC or GLOBALVIEW-CO_2 for the period 2000-2006 is caused mainly by the increasing sinks estimated by the 64-region inversion over the East Asia region (apparently wrongly).

There is often large interannual variability in the differences between sites. For example, the SMO–SPO difference (Fig 2c) seems to be lowest in 1998 and the simulation using INV22_CYC flux successfully reproduces this feature, while the INV22_IAV64 exhibited greater difference. This suggests the emission from the NH tropics is overestimated in INV22_IAV64 flux during the 1997/1998 El Nino. The annual cycle in WPO–GMI difference (Fig 2g) remained small during 1999-2000 and ACTM simulations using both fluxes produce similar features indicating the predominant role of transport. Examination of seasonal cycles at individual sites (not shown here) using GLOBALVIEW-CO_2 time series reveals decreasing and increasing tendency of the seasonal amplitude at GMI and WPO, respectively, from 1997 to 2000. The largest WPO–GMI difference occurred in 1994 due to deep seasonal cycle minimum in October at GMI (which the ACTM failed to simulate) and shallow minimum at WPO. The misfits occur more frequently during the winter/spring for the post-2001 time period as compared to summer/autumn for the pre-1997 period.

The simulation of vertical gradients measured using aircraft has been of interest recently [Stephens et al., 2007]. Figure 2h-j show differences between mid-troposphere and surface CO_2 concentrations at three aircraft profiling sites. The model-observation agreement is generally satisfactory within a few ppm for all months, but the summer time CO_2 uptake given by the model seems to be weaker than what is actually occurring at the surface at the time of measurements (seen as the underestimation of observed differences by the model). This summer-time bias may arise from not including the diurnal cycle in the terrestrial CO_2 flux (because the photosynthetic uptake is strong during the day when the measurements are conducted) or else site representation error in ACTM due to coarse horizontal resolution. It can also be argued that models with thick a boundary layer (due to vigorous vertical mixing) in the summer require unrealistically high uptake for reproducing the measured vertical gradient or vice versa. However, the excellent agreement between the model and measurements of SF_6 at a variety of sites rules out any such transport bias in ACTM [Patra et al., 2009].

3.3. Comparison of CO_2 seasonal cycles and growth rates

The advantage of using INV22_IAV64 over INV22_CYC is for simulating the growth rates of CO_2, which are influenced by decadal scale climate variability, especially in tropical regions [e.g., Rayner et al., 1999; Patra et al., 2005]. The growth rate is the time derivative of the concentration time series with all frequencies shorter than 36 months filtered out, as described in Section 2. Figure 3 shows a Taylor [2001] diagram of correlation coefficient (indicating match in phase of variability) and normalized standard deviation (match in the amplitude of variability), both for seasonal cycle and growth rates as estimated by using the digital filtering technique. The seasonal cycles are well simulated by ACTM at most sites, with average correlation coefficient of 0.90 and normalized standard deviation of 1.0 with respect to GLOBALVIEW-CO_2. We find 3 sites with lowest correlation coefficients to be POCS10, POCS15 and CGO, and 3 sites with highest normalized standard deviations to be BHD, POCS30 and

AMS. These 6 sites with poor model-observation match in seasonal cycle are located in the SH, and the comparisons reveal a too strong seasonal cycle in surface fluxes caused greater seasonal cycle amplitudes in model time series. The interannual variability in growth rate is also captured successfully using INV22_IAV64 flux. Average correlation coefficient and normalized standard deviation are calculated to be 0.73 and 1.09, respectively, over all 139 sites studied here (those are 0.82 and 1.17 for the 103 surface stations, and 0.48 and 0.88 for 36 aircraft profiles, respectively). Low correlation coefficients for the aircraft profile sites are obtained due to large number of missing data in the time series covering a relatively short measurement periods of 4-7 years, because a 36-month filter is applied for calculating the growth rates (ref. Fig. 2h-j).

The model growth rate variabilities are too large by 20% or more (normalized standard deviation > 1.2) compared to GLOBALVIEW-CO_2 growth rate variabilities at 50 sites, which may at first instance indicate that the interannual variability in CO_2 flux is overestimated at regional scales by the 64-region inverse model using NIES/FRCGC forward transport model. Note that both the model residual flux (Fig. 1) and observed growth rate variability are well simulated at MLO (correlation coefficient=0.97, normalized standard deviation=1.07), representing the global average case. Another reason for the overestimation of model growth rate variability relative to that of GLOBALVIEW-CO_2, as seen by the normalized standard deviations, could arise from smoothing of flask data in GLOBALVIEW-CO_2 processing (Masarie and Tans, 1995), while the ACTM simulated concentrations contains the synoptic variability due to transport. Here we hypothesize that if the ACTM results were screened for background condition, as in GLOBALVIEW-CO_2, this comparison would have yielded closer agreement.

For testing this hypothesis, we also compared to the flask data from NOAA ESRL, which were used in producing GLOBALVIEW-CO_2 time series. The main advantage of using flask data is that the model results can be sampled following the time stamp of air sampling, which is a more realistic scenario considering that synoptic scale transport leads to large concentration variations [Patra et al., 2008]. Figure 4 shows the normalized standard deviations generally move closer to the vertical line marked at NSD=1.0 when the ESRL flask data (squares) are used in the analysis compared to those using GLOBALVIEW-CO_2 (circles). Two of the most prominent exceptions are observed for TAP and WLG. The smoothing and interpolation are preferred at WLG due to data gaps or uneven seasonal sampling; e.g., there appears to be more samples in the summer of 2001 and 2002 compared to 2000 and 2003. The TAP site is located in a complex region of CO_2 flux distribution (about 100 km south-west of Seoul city), which cannot be represented well by the coarse-horizontal grid of ACTM (~2.8°x2.8°). Under such circumstances of high site representation error in transport model, GLOBALVIEW-CO_2 is preferred by the ACTM over the actual flask observations.

3.4. Comparison of TransCom mean flux (INV22_CYC) and 64-region inversion flux using ACTM transport (INV64_CYC)

The underestimation of the MLO-SPO CO_2 concentration difference by the ACTM forward simulation using TransCom models derived mean surface flux (Fig. 1c) suggested a bias in the north-south CO_2 sink distribution, i.e., an enhanced NH carbon sink with respect to the SH. It has been noted earlier [Patra et al., 2006] that individual forward transport models need to be improved in order to effectively use atmospheric CO_2 data in source/sink inversions, and estimate CO_2 fluxes with minimal bias. In a suite of forward models, if more models were biased towards slower (faster) vertical transport, the multi-model mean flux would have a bias towards more (less) uptake in the northern mid- and high latitudes, where most number of continental measurement sites are located [Denning et al., 1995; Gurney et al., 2004]. Since ACTM transport is able to simulate inert tracers at annual to synoptic time scales fairly well [Patra et al., 2009], we now used ACTM simulated basis functions for 64-region inversion to derive a CO_2 flux seasonal cycle using GLOBALVIEW-CO_2 for the period of 2000-2002 (INV64_CYC case).

Figure 5 and Table 3 show comparison of latitudinal distribution of INV22_CYC and INV64_CYC (both without the fossil fuel component). As suggested earlier in section 3.1, based on model and GLOBALVIEW-CO_2 comparison of the MLO–SPO concentration difference, the ACTM derived NH-SH flux (INV64_CYC) gradient is indeed weaker by 0.46 PgC yr^{-1} compared to the INV22_CYC (Table 3). Maximum contrasts between these two fluxes are seen for the latitude bands of 45-90^oN (flux difference 0.63 PgC yr^{-1}) and 15-45^oS (flux difference 0.56 PgC yr^{-1}). This bias in INV22_CYC flux is reflected in the ALT (82^{o}N, 63^{o}W)–SMO (14^{o}S, 171^{o}W) concentration difference as the model underestimates GLOBALVIEW-CO_2 values by about 1.0 ppm for most years between 1984-2006 (ref. Fig. S5b), which is greater than what is observed for the MLO–SPO difference. Comparisons of latitude-month distribution of CO_2 fluxes suggest a weaker source and stronger sink in the NH tropics (Equator-15^{o}N) during Feb-May and Aug-Oct months, respectively, by INV64_CYC compared to INV22_CYC (Fig. 5c). Generally a lower land/ocean to atmosphere emission is suggested by INV64_CYC for much of the SH tropics and mid-latitudes during Jan-Mar months. Since the present in situ measurement network is not capable of capturing the CO_2 flux distribution longitudinally at a great confidence, we have restricted our discussion to the latitudinal flux distribution only.

4. Conclusions

We have performed three time-dependent inverse model simulations for (1) cyclostationary fluxes using multiple forward transport models of TransCom-3 (INV22_CYC), (2) interannually varying fluxes using the NIES/FRCGC transport model driven by interannually varying winds (this and case 1 are combined to prepare INV22_IAV64), and (3) cyclostationary fluxes using ACTM (INV64_CYC). Firstly, we confirmed that the variability in the observed airborne fraction of CO_2 is reproduced at inter-decadal time scales using inverse model estimated surface fluxes (INV22_IAV64 case), and there are no apparent trends in airborne fractions over the past three decades. Forward transport simulations using ACTM are used to verify the accuracy of surface fluxes in comparison with an observation-based data product of atmospheric CO_2 at various space and time scales. The transport model (ACTM) has been demonstrated elsewhere [Patra et al., 2009] to model SF_6 distributions accurately. The seasonal cycles, latitude/longitude/altitude gradients, and growth rates are generally well simulated by the forward transport model (i.e., ACTM) and inter-annually varying surface fluxes. The forward simulation is able to reproduce (correlation coefficient > 0.6) the observed seasonal cycles at 134 of the 139 sites with at least 6 years of data coverage over the 1996-2005 period. At 126 of these 139 sites, the observed growth rate variability is simulated statistically significantly (correlation coefficient 0.3; data points > 72), but the amplitude of the variability is somewhat overestimated. Overestimation in seasonal cycle amplitudes in the southern hemispheric sites and overestimation of growth rates variability at some 30% of the sites, as well as underestimation of inter-hemispheric gradient by the ACTM simulation, suggest that further work is required for better constraining the net surface fluxes by inverse modeling. A sensitivity analysis of growth rate variability using the NOAA ESRL flask data in comparison with ACTM simulation of INV22_IAV64 flux showed better agreement than when the GLOBALVIEW-CO_2 data product is used.

The comparison of ACTM forward simulation results to GLOBALVIEW-CO_2 and ESRL observations suggests the GLOBALVIEW-CO_2 product is suitable for flux inversion but is likely to exhibit weaker interannual CO_2 growth rate variability with respect to what can be derived based on in situ observation and transport model simulations driven by interannually varying meteorology. This is because the time scale of atmospheric CO_2 variability is shorter than the surface flux change, particularly at the remote sites. The overall validity of the forward model results is encouraging, and suggests that 3-D datasets of atmospheric CO_2 (and other greenhouse gases) would be useful for climate model analysis if available over a few decades and for meteorological analysis/reanalysis if produced near-real time.

The other significant application of the forward simulation of inversion model fluxes is to validate the net fluxes and flux distribution in latitude and longitude. The horizontal/latitudinal CO_2 concentration differences between MLO–SPO, ALT–SMO and several other tropical sites suggested a bias in mean fluxes derived using multiple forward transport models under the TransCom project (estimates 22-region flux). This bias in latitudinal gradient of net CO_2 flux amount is apparently reduced when a relatively well-validated forward transport model for interhemispheric exchange of SF_6 (ACTM) is used in the 64-region inverse model. The CO_2 sink gradient between the NH and SH latitudes decreased by about 0.46 PgC yr^{-1} in the case of ACTM inversion compared to the TransCom models inversion. We estimated CO_2 fluxes of -0.97, -1.04, 1.64, -2.29 and -0.13 PgC yr^{-1} in the latitude bands 90-45°N, 45-15°N, 15N-15°S 15-45°S and 45-90°S, respectively, using ACTM forward transport. Comparing the 90-15°N and 15-90°S region aggregated fluxes (-2.01 and -2.42 PgC yr^{-1}, respectively, for INV64_CYC, and -2.94 and -1.77 PgC yr^{-1}, respectively, for INV22_CYC), a more dramatic shift of about 1.58 PgC yr^{-1} of uptake from the extratropical north to the south is recommended by the INV64_CYC inversion, compared to those estimated by the INV22_CYC case.

Acknowledgments. The ACTM simulated full set of 3-D distribution and the model time series at sites for the period 1984-2006 can be obtained by contacting the author. This work is partly supported by JSPS/MEXT KAKENHI-A grant number 22241008. We thank the anonymous reviewers and the associate editor for providing us excellent guidance to improve the clarity of the manuscript.

References

Andres, R. J., T. A. Boden, and J. G. Marland (2010), Annual Fossil-Fuel CO_2 Emissions: Mass of Emissions Gridded by One Degree Latitude by One Degree Longitude, *Carbon Dioxide Information Analysis Center, Oak Ridge National Laboratory*, Oak Ridge, U.S.A., doi: 10.3334/CDIAC/ffe.ndp058.2010

Baker, D.F., R. M . Law, K. R. Gurney, A.S. Denning, P.J. Rayner, et al. (2006), Transcom 3 inversion intercomparison: Model mean results for the estimation of seasonal carbon sources and sinks, *Global Biogeochem. Cycles, 18*, GB1010.

Boden, T.A., G. Marland, and R. J. Andres (2009), Global CO_2 emissions from fossil-fuel burning, cement manufacture, and gas flaring: 1751-2006, *Carbon Dioxide Information Analysis Center*, Oak Ridge Natl. Lab., Oak Ridge, Tennessee.

Brenkert, A. L. (1998), Carbon Dioxide Emission Estimates from Fossil-Fuel Burning, Hydraulic Cement Production, and Gas Flaring for 1995 on a One Degree Grid Cell Basis, *Carbon Dioxide Information Analysis Center, Oak Ridge National Laboratory*, Oak Ridge, U.S.A., doi: 10.3334/CDIAC/ffe.ndp058.2003.

Buermann, W., B. R. Lintner, C. D. Koven, A. Angert, J. E. Pinzon||, C. J. Tucker, and I. Y. Fung (2007), The changing carbon cycle at Mauna Loa Observatory, *Proc. Nat. Acad. Sci. (USA), 104*, 4249-4254.

Canadell, J.G., C. Le Quéré, M. R. Raupach, C. B. Field, E. T. Buitenhuis, P. Ciais, T. J. Conway, N. P. Gillett, R. A. Houghton, and G. Marland (2007), Contributions to accelerating atmospheric CO_2 growth from economic activity, carbon intensity, and efficiency of natural sinks, *Proc. Nat. Acad. Sci. (USA), 104*, 18866-18870.

Chevallier, F., et al. (2010), CO_2 surface fluxes at grid point scale estimated from a global 21 year reanalysis of atmospheric measurements, J. Geophys. Res. , 115 , D21307, doi:10.1029/2010JD013887.

Conway, T., P. Tans, L. Waterman, K. Thoning, D. Kitzis, K. Masarie, and N. Zhang (1994), Evidence for interannual variability of the carbon cycle from the National Oceanic and Atmospheric Administration/Climate Monitoring and Diagnostics Laboratory Global Air Sampling Network, *J. Geophys. Res., 99*(D11), 22831-22855.

Denning, A. S., I. Y. Fung, D. Randall (1995), Latitudinal gradient of atmospheric CO_2 due to seasonal exchange with land biota, *Nature, 376*, 240-243.

EDGAR4 (2009), European Commission, Joint Research Centre (JRC)/Netherlands Environmental Assessment Agency (PBL), Emission Database for Global Atmospheric Research (EDGAR), release version 4.0. http://edgar.jrc.ec.europa.eu.

Geller, L.S., J. W. Elkins, J. M. Lobert, A. D. Clarke, D. F. Hurst, J. H. Butler, and R. C. Myers (1997), Tropospheric SF_6: Observed latitudinal distribution and trends, derived emissions and interhemispheric exchange time, *Geophys. Res. Lett., 24*(6), 675-678.

GLOBALVIEW-CO_2 (2009), Cooperative Atmospheric Data Integration Project - Carbon Dioxide. CD-ROM, NOAA CMDL, Boulder, Colorado [anonymous FTP to ftp.cmdl.noaa.gov, path: ccg/CO2/GLOBALVIEW].

Gregg , J. S., R. J. Andres, and G. Marland (2008), China: Emissions pattern of the world leader in CO_2 emissions from fossil fuel consumption and cement production, Geophys. Res. Lett., 35, L08806.

Gu, L., D. D. Baldocchi, S. C. Wofsy, J. W. Munger, J. J. Michalsky, S. P. Urbanski, and T. A. Boden (2003), Response of a deciduous forest to the Mount Pinatubo eruption: Enhanced photosynthesis, *Science, 299*, 2035-2038.

Gurney, K. R., R. M. Law, P. J. Rayner, and A. S. Denning, TransCom-3 experimental protocol, *Paper No. 707*, Dept. Atmos. Sci., Colo. State Univ., 2000.

Gurney, K.R., R. M. Law, K. R. Gurney, A. S. Denning, P. J. Rayner, et al. (2004), Transcom 3 inversion intercomparison: Model mean results for the estimation of seasonal carbon sources and sinks, *Global Biogeochem. Cycles, 18*, GB1010.

Higuchi, K., S. Murayama, and S. Taguchi (2002) Quasi-decadal variation of the atmospheric CO_2 seasonal cycle due to atmospheric circulation changes: 1979–1998, *Geophys. Res. Lett., 29*(8), 1173

Houghton, R.A. (2003), Revised estimates of the annual net flux of carbon to the atmosphere from changes in land use and land manangement 1850-2000, *Tellus, 55B*, 378-390.

Keeling, C. D., R. B. Bacastow, A. F. Carter, S. C. Piper, T. P. Whorf, M. Heimann, W. G. Mook, and H. Roeloffzen (1989), A Three Dimensional Model of Atmospheric CO_2 Transport Based on Observed Winds: 1. Analysis of Observational Data, in Aspects of Climate Variability in the Pacific and the Western Americas, edited by D. H. Peterson, American Geophysical Union, Washington, D.C., pp. 165-236.

Keeling, C.D., J. F. S. Chin, and T. P. Whorf (1996) Increased activity of northern vegetation inferred from atmospheric CO_2 measurements, *Nature 382*, 146-149.

Keeling, R.F., S. C. Piper, and M. Heimann (1996a), Global and hemispheric CO_2 sinks deduced from changes in atmospheric O_2 concentration, *Nature, 381*, 218-221.

Khatiwala, S., F. Primeau, and T. Hall (2009), Reconstruction of the history of anthropogenic CO_2 concentrations in the ocean, *Nature, 462*, doi: 10.1038/nature08526.

Law, R. M., W. Peters, C. Rodenbeck, et al. (2008), TransCom model simulations of hourly atmospheric CO_2: experimental overview and diurnal cycle results for 2002, *Global Biogeochem. Cycles, 22*, GB3009.

Lucht, W., I. C. Prentice, R. B. Myneni, S. Sitch, P. Friedlingstein, W. Cramer, P. Bousquet, W. Buermann, and B. Smith (2002), Climatic control of the high-Latitude vegetation greening trend and Pinatubo effect, *Science, 296*, 1687-1689.

Maksyutov, S., P. K. Patra, R. Onishi, T. Saeki, T. Nakazawa (2008), NIES/FRCGC global atmospheric tracer transport model: Description, validation, and surface sources and sinks inversion, *J. Earth Simulator, 9*, 3–18.

Masarie, K., and P. Tans (1995), Extension and integration of atmospheric carbon dioxide data into a globally consistent measurement record, *J. Geophys. Res., 100*(D6), 11593-11610.

Nakazawa, T., M. Ishizawa, K. Higuchi, and N. B. A. Trivett (1997), Two curve fitting methods applied to CO_2 flask data, *Environmetrics, 8*, 197-218.

Numaguti, A., M. Takahashi, T. Nakajima, and A. Sumi (1997), Development of CCSR/NIES atmospheric general circulation model, in Reports of a New Program for Creative Basic Research Studies, *CGERs Supercomput. Monogr. Rep., 3*, 1-48, CGER, Tsukuba, Ibaraki.

Patra, P. K., S. Maksyutov, and T. Nakazawa (2005), Analysis of atmospheric CO_2 growth rates at Mauna Loa using inverse model derived CO_2 fluxes, *Tellus, 57B*, 357-365.

Patra, P. K., K. R. Gurney, et al., Sensitivity of inverse estimation of annual mean CO_2 sources and sinks to ocean-only sites versus all-sites observational networks, Geophys. Res. Lett., 33, L05814, 2006.

Patra, P. K., R. M. Law, W. Peters, C. Rodenbeck, M. Takigawa, et al. (2008), TransCom model simulations of hourly atmospheric CO_2: analysis of synoptic scale variations for the period 2002-2003, *Global Biogeochem. Cycles, 22*, GB4013.

Patra, P. K., M. Takigawa, G. S. Dutton, K. Uhse, K. Ishijima, B. R. Lintner, K. Miyazaki, and J. W. Elkins (2009), Transport mechanisms for synoptic, seasonal and interannual SF_6 variations and "age" of air in troposphere, *Atmos. Chem. Phys., 9*, 1209-1225.

Peters, W., A. Jacobson, C. Sweeney, A. Andrews, T. Conway, K. Masarie, et al. (2007), An atmospheric perspective on North American carbon dioxide exchange: CarbonTracker, *Proc. Natl. Acad. Sci (USA)*, 104, 48, 18925–18930.

Randerson, J., M. Thompson, T. Conway, I. Fung, and C. Field (1997), The contribution of terrestrial sources and sinks to trends in the seasonal cycle of atmospheric carbon dioxide, *Global Biogeochem. Cycles, 11*(4), 535-560.

Rayner, P. J., I. G. Enting, R. J. Francey, and R. Langenfelds (1999), Reconstructing the recent carbon cycle from atmospheric CO_2, ^{13}C and O_2/N_2 observations, *Tellus, 51B*, 213-232.

Stephens, B. B., K. R. Gurney, P. P. Tans, C. Sweeney, et al. (2007), Weak northern and strong tropical land carbon uptake from vertical profiles of atmospheric CO_2, *Science, 316*, 1732–1735.

Tans, P. P., I. Y. Fung, and T. Takahashi (1990), Observational Constraints On the Global Atmospheric CO_2 Budget, *Science, 247*, 1431-1438.

Taylor, K. E. (2001), Summarizing multiple aspects of model performance in single diagram, *J. Geophys. Res., 106*(D7), 7183-7192.

Takahashi, T., S. C. Sutherland, C. Sweeney, A. Poisson, N. Metzl, B. Tilbrook, N. Bates, R. Wanninkhof, R. A. Feely, C. Sabine, J. Olafsson, and Y. Nojiri (2002), Global sea-air CO_2 flux based on climatological surface ocean pCO_2, and seasonal biological and temperature effects, *Deep-Sea Research Part II, 49*, 1601-1622.

Tohjima, Y., H. Mukai, S. Hashimoto, and P. K. Patra (2010), Increasing synoptic scale variability in atmospheric CO_2 at Hateruma Island associated with increasing East-Asian emissions, *Atmos. Chem. Phys., 10*, 453-462.

Table 1: Summary of inversion fluxes and corresponding forward transport models as used in this study (see text for details). Note that all forward transport simulations are made using ACTM only for comparison with atmospheric CO_2 time series ESRL measurements or GLOBALVIEW-CO_2 data product, while different forward transport models are employed for flux inversions. When the INV64_CYC fluxes are used in forward simulations, it is referred to as 'recursive' method (ref. section 3.5).

Inverse flux code	CO_2 data	Forward transport model	Further information
INV22_CYC	2000-2002; 87 sites	12 models from TransCom (Level 3) using one year of meteorology (cyclostationary)	22 region inversion for monthly-mean fluxes as in TransCom but for different period and data network
INV22_IAV64	1979-2006; 26 sites or 80 sites	NIES/FRCGC CTM with interannually varying (IAV) meteorology	Monthly-mean flux anomalies for 1979-2006 from 64-region inversion added to INV22_CYC
INV64_CYC	2000-2002; 92 sites	ACTM; forward transport validated using SF_6	Same as INV22_CYC, but for 64-region inversion

Table 2: Airborne fractions (AFs) and atmospheric burden (AB; within parenthesis) for different decades as estimated from two inversion fluxes (fossil added) and MLO growth rate (ref. Fig. 1 caption).

Time Period	**AF (in %) or AB (PgC yr^{-1})**			**FOS emission (PgC yr^{-1})**
	INV22_CYC	**INV22_IAV64**	**MLO_GR**	
1984-1989	48 (2.71)	59 (3.34)	61 (3.47)	5.7
1990-1999	53 (3.38)	52 (3.29)	50 (3.18)	6.35
2000-2006	60 (4.45)	58 (4.29)	57 (4.23)	7.39
1984-2006	54	56	55	

Table 3: Comparison of non-fossil CO_2 fluxes for the time period of 2000-2002 as estimated by the INV22_CYC and INV64_CYC inversion cases, aggregated over broad latitude bands. Note that the 22/64-region inversion fluxes are distributed to $1^o \times 1^o$ grid of the earth's surface and then the aggregated fluxes for different latitude band are calculated.

Hemisphere	TransCom	ACTM	Latitude band	TransCom	ACTM
			90^oN-45^oN	-1.608	-0.974
Northern	-1.91	-1.68	45^oN-15^oN	-1.335	-1.040
			15^oS-15^oN	1.913	1.637
Southern	-0.88	-1.11	15^oS-45^oS	-1.726	-2.286
			45^oS-90^oS	-0.046	-0.135

Figure Captions

Figure 1: (a) Time series of MLO CO_2 growth rate (source: NOAA ESRL; www.esrl.noaa.gov/gmd/ccgg/trends/#mlo_growth; converted to residual flux by assuming 1.0 ppm = 2.12 PgC; 1Pg = 10^{15}g) and other flux variabilities for the period of 1983-2006. Emission due to landuse/landuse change (LULUC) is taken from Houghton [2003]. ACTM simulated CO_2 concentrations time series for MLO and SPO are shown in panel (b). Differences in concentrations between MLO and SPO as simulated by ACTM corresponding to two inversion fluxes are shown in comparisons with GLOBALVIEW-CO_2 (panel c).

Figure 2: Meridional (a,b,c,d), zonal (e,f) and vertical (g, h, i, j) gradients in monthly-mean atmospheric CO_2 concentrations between selected observation sites for the period 1994-2006. The GLOVALVIEW-CO_2 abbreviated site names and location are given in the title of each panel. The sites used in panels a-f are located on the earth's surface, WPO at aircraft cruising altitude of ~10 km and GMI at surface (f), and the rest (h-j) used data from 500 m (***005; where *** is site name; 1500 m for PFA) and 5500 m (***055) from aircraft profile measurements. Note the y-axis range differs for each panels.

Figure 3: Taylor [2001] diagram showing the model performance for simulating seasonal cycle (SC) and growth rate (GR) of CO_2 at 103 surface stations (surf) and 36 profiles (prof) time series corresponding to the INV22_IAV64 flux (see text). For perfect model-observation match, symbol will fall on 1 of the horizontal axis. Note here that while most of the surface sites were used in inversion, the profiles were not, and thus should be treated as independent data for flux validation.

Figure 4: Comparison normalized standard deviations of growth rate as estimated using the GLOBALVIEW-CO_2 data product and NOAA ESRL flask observations at 29 sites (three letter site codes are given only with square symbols).

Figure 5: Comparison of non-fossil fluxes as estimated by 22-region inversion using the TransCom models' transport (12 model mean) and 64-region inversion using ACTM transport for the period 2000-2002. All regional fluxes estimated by inversion are first distributed at 1x1 degree resolution following the basis function maps and added to the terrestrial and oceanic presubtracted fluxes. The values plotted here are after zonal aggregation of those for each of the latitudes (units: million of g-C degree-latitude^{-1} s^{-1}).

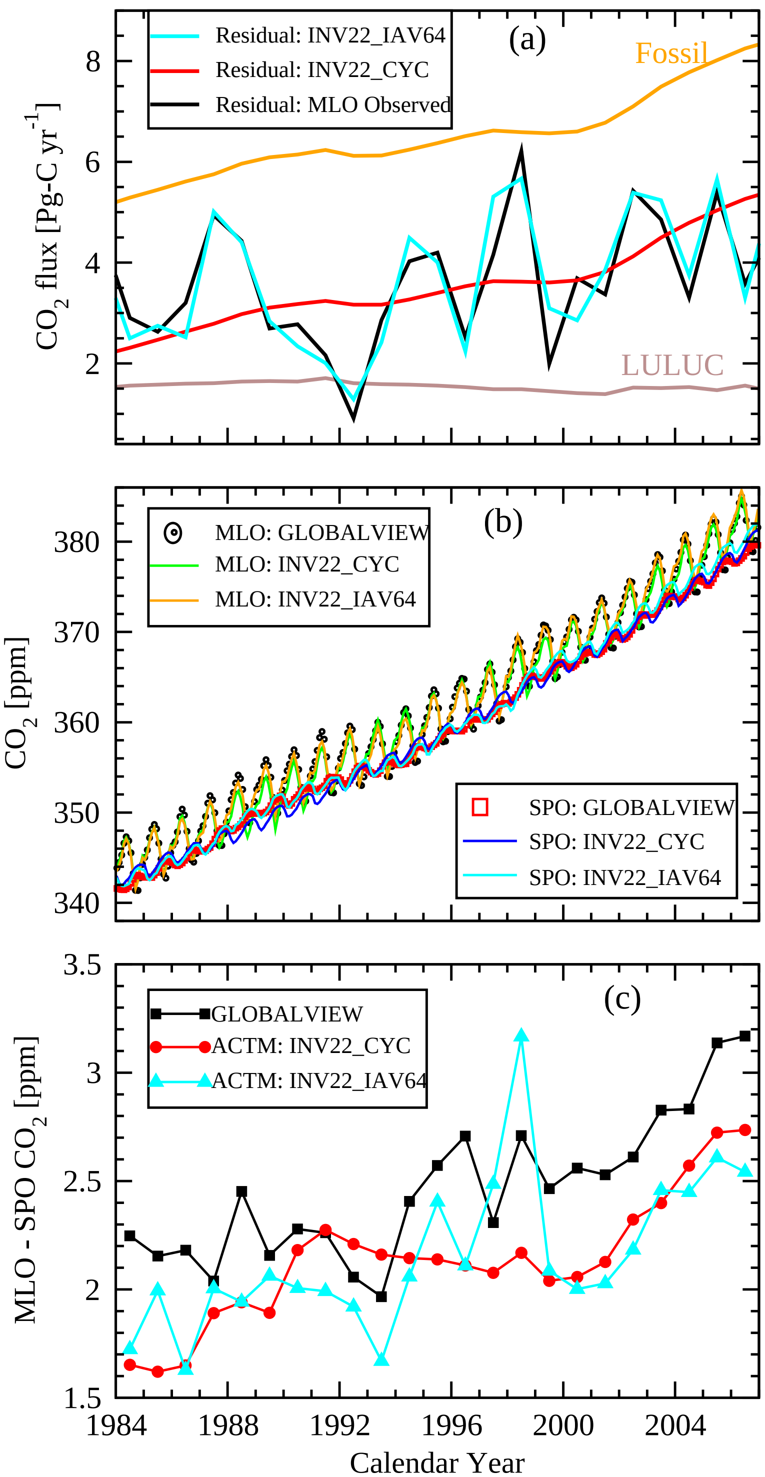

(a)
Residual: INV22_IAV64
Residual: INV22_CYC
Residual: MLO Observed
Fossil
LULUC
CO2 flux [Pg-C yr-1]
(b)
MLO: GLOBALVIEW
MLO: INV22_CYC
MLO: INV22_IAV64
SPO: GLOBALVIEW
SPO: INV22_CYC
SPO: INV22_IAV64
CO2 [ppm]
(c)
GLOBALVIEW
ACTM: INV22_CYC
ACTM: INV22_IAV64
MLO - SPO CO2 [ppm]
Calendar Year

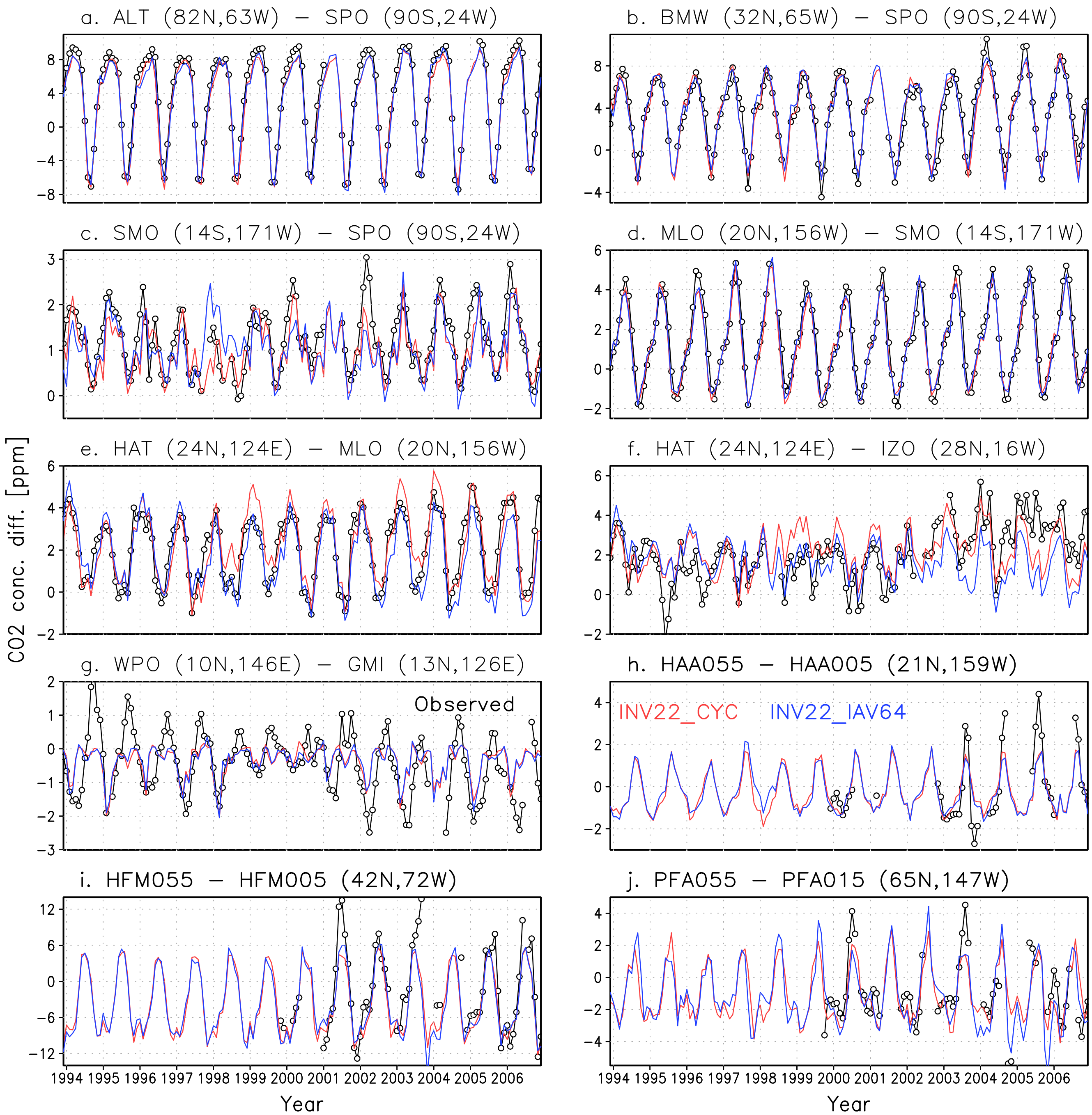

a. ALT (82N,63W) – SPO (90S,24W)
b. BMW (32N,65W) – SPO (90S,24W)
c. SMO (14S,171W) – SPO (90S,24W)
d. MLO (20N,156W) – SMO (14S,171W)
e. HAT (24N,124E) – MLO (20N,156W)
f. HAT (24N,124E) – IZO (28N,16W)
g. WPO (10N,146E) – GMI (13N,126E)
h. HAA055 – HAA005 (21N,159W)
i. HFM055 – HFM005 (42N,72W)
j. PFA055 – PFA015 (65N,147W)
Observed
INV22_CYC
INV22_IAV64
CO2 conc. diff. [ppm]
Year
1994 1995 1996 1997 1998 1999 2000 2001 2002 2003 2004 2005 2006

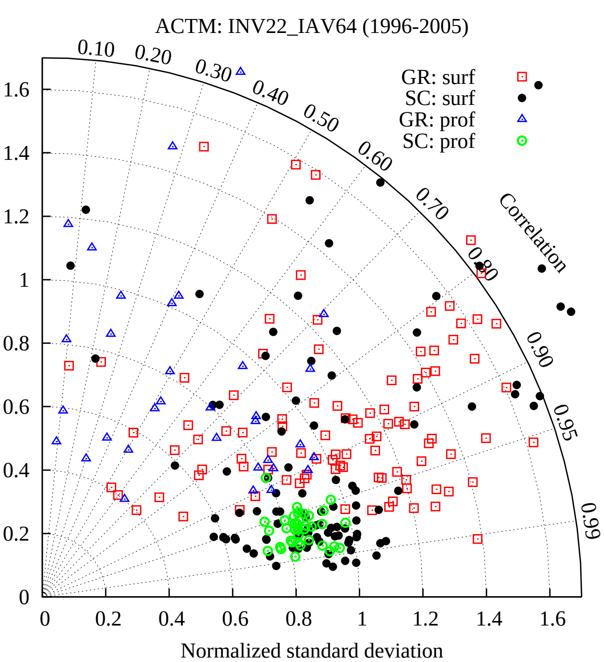
ACTM: INV22_IAV64 (1996-2005)
GR: surf
SC: surf
GR: prof
SC: prof
Correlation
0.10
0.20
0.30
0.40
0.50
0.60
0.70
0.80
0.90
0.95
0.99
0
0.2
0.4
0.6
0.8
1
1.2
1.4
1.6
Normalized standard deviation

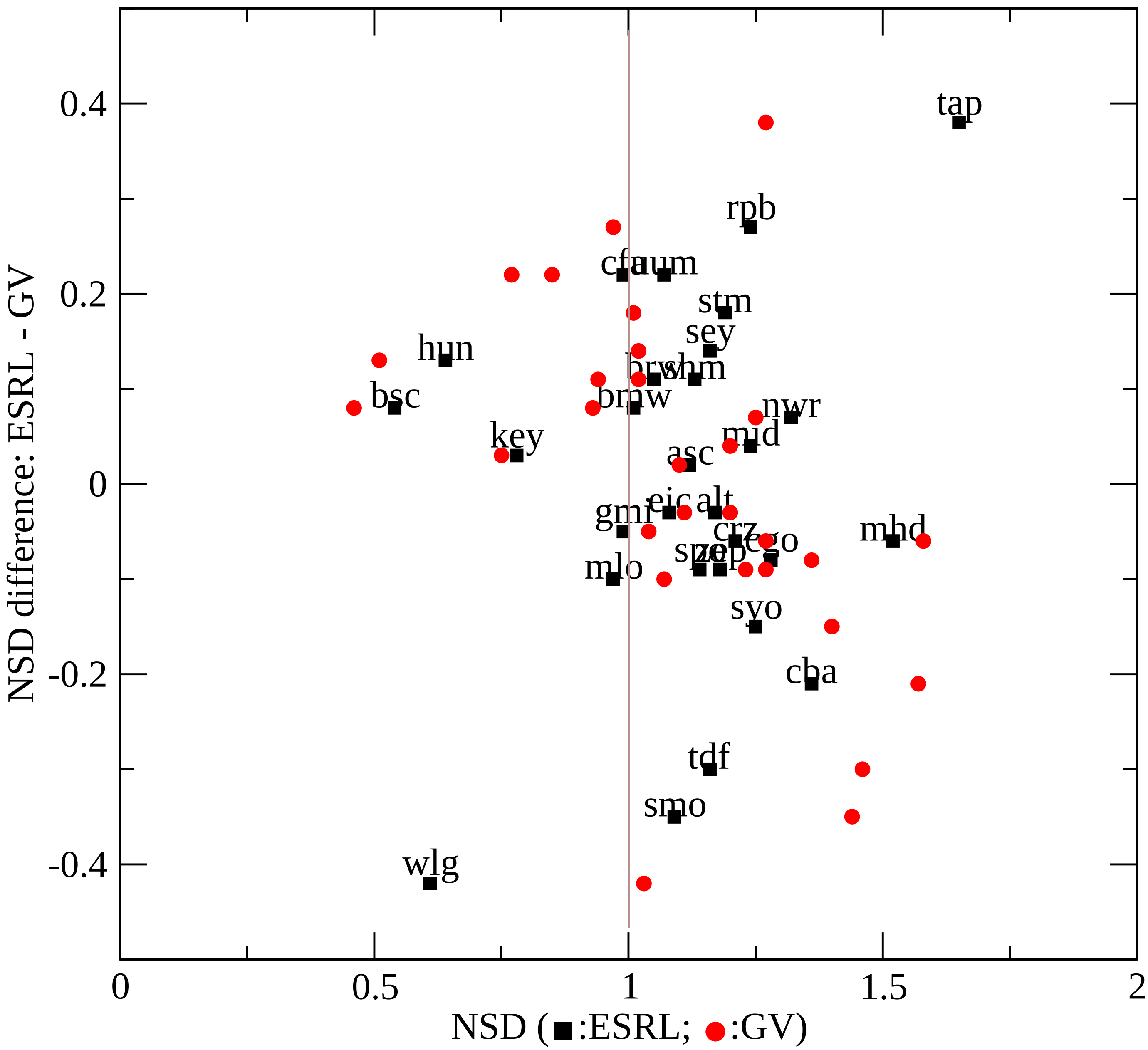
NSD difference: ESRL - GV
NSD (■:ESRL; ●:GV)
0.4
0.2
0
-0.2
-0.4
0
0.5
1
1.5
2
tap
rpb
cfa
aum
stm
sey
hun
brw
shm
bsc
bmw
nwr
key
mid
asc
gmi
eic
alt
mhd
crz
cgo
spo
zep
mlo
syo
cba
tdf
smo
wlg

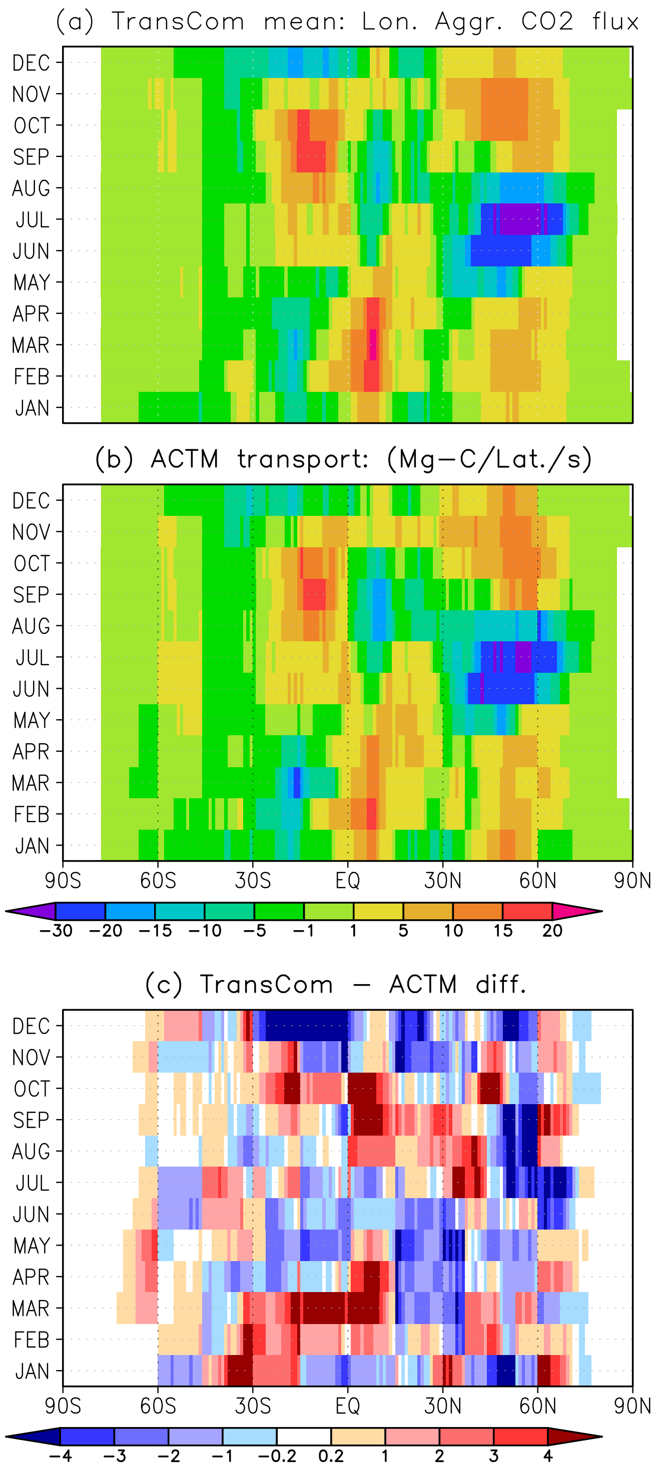
(a) TransCom mean: Lon. Aggr. CO2 flux
DEC
NOV
OCT
SEP
AUG
JUL
JUN
MAY
APR
MAR
FEB
JAN
(b) ACTM transport: (Mg−C/Lat./s)
90S
60S
30S
EQ
30N
60N
90N
−30
−20
−15
−10
−5
−1
1
5
10
15
20
(c) TransCom − ACTM diff.
−4
−3
−2
−1
−0.2
0.2
1
2
3
4